

## A Study of Thunderstorm Microphysics with Multiparameter Radar and Aircraft Observations

E. A. BRANDES, J. VIVEKANANDAN, J. D. TUTTLE, AND C. J. KESSINGER

*National Center for Atmospheric Research, Boulder, Colorado*

(Manuscript received 2 December 1994, in final form 30 May 1995)

### ABSTRACT

Excellent agreement was found between multiparameter radar signatures of hail, raindrops, and mixed-phase precipitation and in situ precipitation particle measurements made by aircraft in a northeastern Colorado hailstorm. Radar reflectivity estimates determined by remote measurement and from observed particle distributions generally agreed within 5 dB. Maximum values of differential reflectivity ( $Z_{DR}$ ) and the fractional contribution of liquid water to total reflectivity ( $f_{rain}$ ) differed by less than 0.8 dB and a factor of 2, respectively.

A positive  $Z_{DR}$  column, which extended more than 2 km above the freezing level, was nearly coincident with the storm updraft. The column contained mixed-phase precipitation, but the  $Z_{DR}$  measurement was dominated by a small number of very large raindrops (some exceeding 5 mm in diameter). Trajectories computed with a precipitation growth model suggest that many drops originated with partially or totally melted particles from a quasi-stationary feeder band within the inflow region of the storm. The terminal velocity of the drops composing the  $Z_{DR}$  column exceeded updraft speeds, and therefore, they may have simply fallen from the storm. Although particle observations and radar measurements in the column at approximately 3 km AGL and a temperature of  $-2^{\circ}\text{C}$  revealed that the fractional contribution of drops to radar reflectivity was roughly 0.5–0.8, the concentration of supercooled water represented by the drops (a maximum of  $0.5\text{ g m}^{-3}$  and an average of  $0.2\text{ g m}^{-3}$ ) was about half that associated with cloud water. Hence, the relative importance of the large drops and consequently that of the  $Z_{DR}$  column as a source of hail embryos, and a factor in hail growth, may have been minor.

### 1. Introduction

Multiparameter radars, that is, radars making both polarimetric and multiwavelength measurements, are capable of discriminating between mixed-phase and homogeneous precipitation types. Polarimetric radar signatures depend on the mean values and distributions of size, shape, and spatial orientation as well as the composition (dielectric constant) of particles filling the radar resolution volume. Hail, graupel, snow, and rain have distinctive electromagnetic scattering properties and characteristic signatures in the backscattered energy. [See, e.g., Doviak and Zrníć (1984) for a review of the subject.] Multiwavelength radar systems exploit geometric relationships between hydrometeor size and radar wavelength.

Previous investigators have uncovered distinct signatures for raindrops (Seliga and Bringi 1976), mixed-phase precipitation (Herzogh and Jameson 1992), hail and graupel (Bringi et al. 1984; Illingworth et al. 1986; Bringi et al. 1986; Aydin et al. 1986; Tuttle et al. 1989), and large hail (Eccles and Atlas 1973; Bringi et al. 1986). By combining signatures, the three-dimensional distributions of dominant particle types

within precipitating systems can be determined (e.g., Zrníć et al. 1993).

To evaluate techniques for the detection of hail, multiparameter radar measurements were obtained with the National Center for Atmospheric Research (NCAR) CP-2 radar during the summers of 1992 and 1993. In this preliminary study, radar signatures of particle type are verified by comparison with in situ particle measurements made by research aircraft. The radar signatures, radar-derived storm flow, and the precipitation growth model of Knight and Knupp (1986) are then used to study hail production within the storm. A prominent storm feature, often seen in convective storms, is a columnar region of large drops that extended well above the freezing level (see, e.g., Caylor and Illingworth 1987; Illingworth et al. 1987; Tuttle et al. 1989; Meischner et al. 1991; Conway and Zrníć 1993; Tuttle 1993). Possible sources of the drops and their importance to hail production are examined.

### 2. Database

#### *a. Radar parameters and observations*

Precipitation-type discrimination is founded on the observations that raindrops tend to flatten as they fall, increasing in flatness as their size increases, and that hail, graupel, and aggregates tend to tumble and to fall

Corresponding author address: Dr. Edward A. Brandes, NCAR, P.O. Box 3000, Boulder, CO 80307-3000.

TABLE 1. Typical multiparameter values of differential reflectivity  $Z_{DR}$  and linear depolarization ratio LDR for homogeneous distributions of various precipitation particles [taken from Vivekanandan et al. (1993) at S band].

Precipitation type	$Z_{DR}$ , (dB)	LDR (dB)
Rain	0.5 to 4.0	-30 to -24
Graupel	~0.4	-25 to -19
Dry hail	~ -0.5	-23 to -11
Wet hail	-1.0 to -0.5	~ -22
Aggregates	~0	-25 to -20
Columns	2 to 5	-30 to -15*
Plates	4 to 8	-30
Needles	2 to 3	-30 to -15*

\* Dependent upon the antenna elevation angle.

with random orientation. Pristine frozen particles such as columns, plates, and needles are thought to fall with a preferred orientation and have characteristic radar signals that are sensitive to their mean canting angle.

The differential reflectivity (Seliga and Bringi 1976), defined as the ratio of reflectivity at horizontal ( $Z_H$ ) and vertical ( $Z_V$ ) polarizations—that is,  $Z_{DR} \equiv 10 \times \log(Z_H/Z_V)$ —has particular import for particle type discrimination.<sup>1</sup> The flattening of raindrops causes  $Z_{DR}$  to be positive for rain. Magnitudes depend on the median size of the drops; typical values at S band (taken from Vivekanandan et al. 1993) are between 0.5 and 4 dB (see Table 1).

For precipitation particles that tumble,  $Z_{DR}$  is approximately zero. Differential reflectivity is insensitive to fluctuations in drop size distributions (Golestani et al. 1989). Hence, departures from the expected rain relationship indicate the presence of nonaligned ice particles (cf. rain and hail, Table 1). The collocation of small  $Z_{DR}$  and high  $Z_H$  indicates hail (Bringi et al. 1986). On occasion, large hail may fall with its major axis in the vertical (Knight and Knight 1970; Steinhorn and Zrnić 1988), and  $Z_{DR}$  values may be less than zero. Typical values for other particle types are also given in Table 1.

A variation of the  $Z_{DR}$  hail detection method, described by Aydin et al. (1986), defines a differential reflectivity hail signal  $H_{DR} [\equiv Z_H - f(Z_{DR})]$ , where

$$f(Z_{DR}) = \begin{cases} 27 \text{ dB}, & Z_{DR} \leq 0 \text{ dB} \\ 19Z_{DR} + 27 \text{ dB}, & 0 \leq Z_{DR} \leq 1.74 \text{ dB} \\ 60 \text{ dB}, & Z_{DR} > 1.74 \text{ dB}. \end{cases}$$

The empirically determined boundary  $f(Z_{DR})$  delineates pure rain from mixed-phase precipitation. Regions with positive  $H_{DR}$ , marked with strong gradi-

ents at their edges, signify the presence of ice particles. The greater the value of  $H_{DR}$  the greater the likelihood that ice is present.

In this study,  $H_{DR}$  is used to discriminate between rain-only and mixed-phase precipitation. The rain-only measurements were used, following the methodology of Golestani et al. (1989), to compute the fractional contribution of raindrops to  $Z_H$ . First, a sample of 226 paired  $Z_H$  and  $Z_{DR}$  measurements from a low elevation scan ( $0.5^\circ$ ) was tabulated (Fig. 1). In the figure, the segmented line depicts  $f(Z_{DR})$  and separates mixed-phase from rain-only measurements. Golestani et al. define a difference reflectivity  $Z_{DP}$ , where

$$Z_{DP} = 10 \log(Z_H - Z_V) \text{ dBZ}$$

and  $Z_H > Z_V$ . The difference reflectivity for those points in Fig. 1 with  $H_{DR} < 0$  (186 total points) are plotted against  $Z_H$  in Fig. 2. A linear least squares fit to the points yields

$$Z_{DP} = -6.97 + 1.07Z_H \text{ dBZ}.$$

This relationship is similar to that found by Conway and Zrnić (1993) for another northeastern Colorado storm.

If ice particles tumble and have no preferred orientation, then  $Z_{H,ice} = Z_{V,ice}$ . In that case, measured values of  $Z_{DP}$  are due to rain alone and

$$Z_{DP} = -6.97 + 1.07Z_{H,rain} \text{ dBZ}.$$

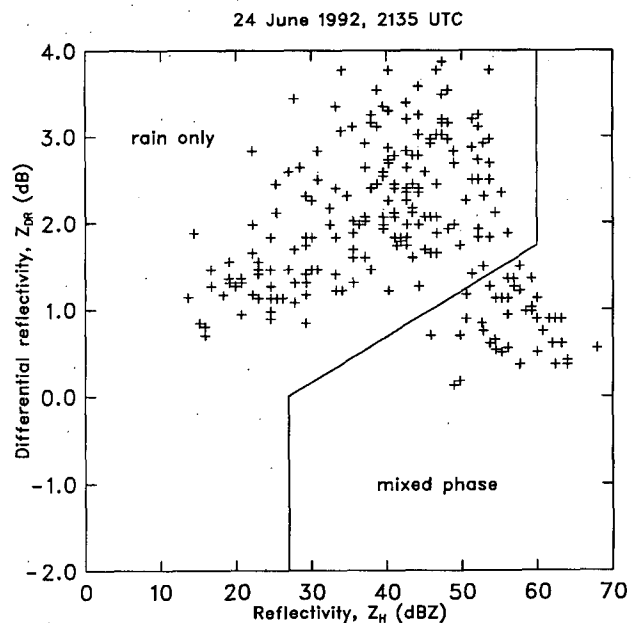


FIG. 1. The distribution of radar reflectivity factor at horizontal polarization  $Z_H$  plotted versus differential reflectivity  $Z_{DR}$  for 226 uniformly spaced measurements from a  $0.5^\circ$  elevation scan obtained at 2135 UTC 24 June 1992. Overplots are not distinguishable. The segmented line represents the function  $f(Z_{DR})$ . Measurements to the right of the line imply the presence of hail.

<sup>1</sup> Unless otherwise noted, measurements are made at S band (10.7-cm wavelength). [A technical description of the NCAR CP-2 multiparameter radar is given by Keeler et al. (1989).]

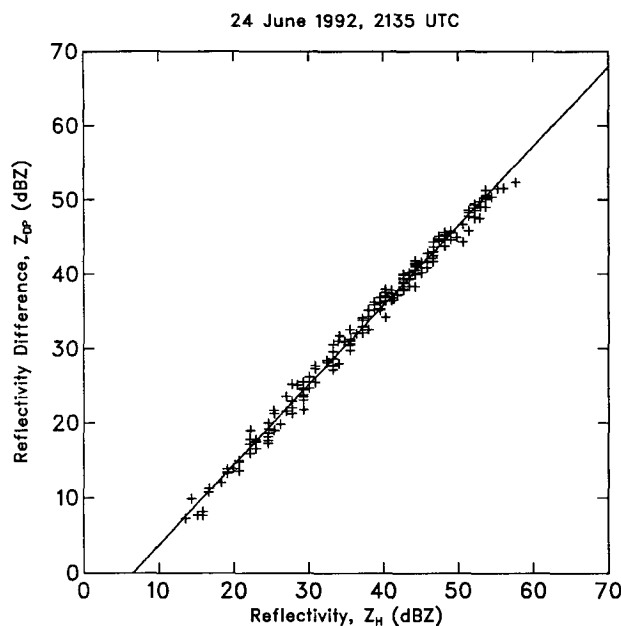


FIG. 2. The distribution of radar reflectivity factor at horizontal polarization  $Z_H$  plotted versus reflectivity difference  $Z_{DP}$  for 186 points in Fig. 1 with  $H_{DR} > 0$ . The region to the right of the line represents mixed-phase precipitation.

In mixed-phase precipitation the fractional contribution of raindrops to the total reflectivity is

$$f_{\text{rain}} = \frac{Z_{H,\text{rain}}}{Z_H} \quad (\text{linear units}).$$

Some of the scatter in Fig. 2 is due to the standard deviation in the radar measurements of  $Z_H$  and  $Z_{DR}$  (1 and 0.2 dB, respectively). (Measurements obviously contaminated by ground targets were rejected outright.) For those points to the left of the line,  $f_{\text{rain}} > 1$ . In fact, for some displayed points  $f_{\text{rain}}$  approaches 1.6. Values greater than 1 were set to 1. The loss of these statistical fluctuations means that areal averages of  $f_{\text{rain}}$  are always less than 1. Similarly, the constraint that  $Z_H > Z_V$  dictates that averages of  $f_{\text{rain}}$  are greater than 0. Hence,  $f_{\text{rain}}$ , as used in this study, is biased toward moderate values.

The linear depolarization ratio (e.g., Herzegh and Jameson 1992), LDR [ $\equiv 10 \log(Z_{HV}/Z_{HH})$ ], is determined by transmitting horizontally polarized radar signals and measuring both horizontally and vertically polarized echoes. When nonspherical particles are illuminated by the radar beam, a portion of the incident horizontally polarized wave is depolarized and scattered into the vertical direction. Factors determining the amount of depolarization are the precipitation phase, the mean shape of the particles, their mean canting angle, and the elevation of the antenna. This measurement is made at X band (3.2-cm wavelength). Heavy rainfall and the increased flattening of raindrops as median drop sizes increase causes  $Z_{HV}$  and  $Z_{HH}$  signals to be

attenuated differentially. Corrections are applied using the scheme of Tuttle and Rinehart (1983) with the assumption that the attenuation of the returned cross-polarized signal is proportional to that of the horizontally polarized signal. The procedure does not account for all signal losses, and a bias often results. Affected regions are readily identified by a progressive increase in LDR (Herzegh and Jameson 1992). Typical LDR values for various particle types are given in Table 1.

For hail detection a dual-wavelength ratio DWR [ $\equiv 10 \log(Z_S/Z_X)$ ] is computed, where  $Z_S$  and  $Z_X$  are horizontally polarized reflectivity measurements at S and X band. The technique, proposed by Atlas and Ludlam (1961), makes use of the differences in scattering that arise at different radar wavelengths. Corrections, which at best are approximate, must be made for the attenuation by rain at X band. Again, the methodology used is that of Tuttle and Rinehart (1983). Hail signatures depend on the size and composition (whether wet, dry, or spongy). A DWR value of greater than 3 dB indicates hail larger than 1 cm in diameter (see, e.g., Battan 1973, Fig. 10.7). DWR is an unambiguous hail signature, if rainfall attenuation is properly compensated. Experience shows that obvious correction errors typically involve hail falls or low antenna elevation angles where blockage (ground targets) causes differential signal loss.

The CP-2 radar was operated continuously, sampling alternately in horizontal and vertical sector-scanning modes. The time interval between volumetric scans was about 3 min. Measurements from the Mile High Radar were used for surveillance and provided dual-Doppler capability in postanalysis. The analysis technique is described in Brandes (1977) with the added constraint that the vertical velocity be zero at the ground and at the storm top. The relative location of the radars is shown in Fig. 3. The small angle between the radar beams ( $\sim 30^\circ$ ), the great distances from the radars ( $\sim 70$  km), and the beam broadening that occurs at these ranges make the storm marginal for dual-Doppler analysis (e.g., Ray and Wagner 1976; Davies-Jones 1979) and result in considerable aliasing of small-scale features. Also, significant evolution of small-scale features is likely to have occurred over the time window in which the data were collected (2135:50–2142:30).<sup>2</sup>

#### b. Verification data

An important part of the field program was the collection of in situ verification data. Ground observations of precipitation were made by two chase vehicles directed by radio communication to suspected hail shafts, as determined from radar measurements. Recorded observations included the time and location of the precip-

<sup>2</sup> All times are UTC; all heights are AGL.

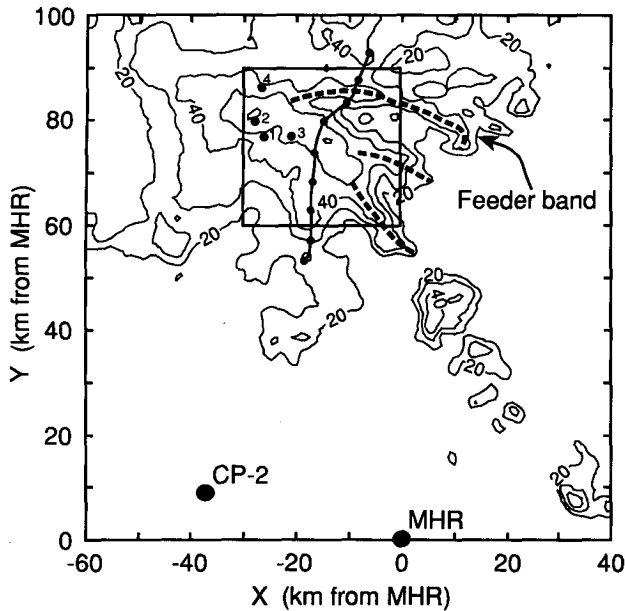


FIG. 3. Map showing the relative location of the multiparameter radar (CP-2), the MHR, and the storm complex as portrayed by radar reflectivity measurements from MHR at 2137 UTC 24 June 1992 ( $1.2^\circ$  antenna elevation) projected onto a rectangular grid with 0.5-km grid spacing. Low-level bands of reflectivity described in the text are marked by heavy dashed lines. The small square shows the location of the dual-Doppler analysis. Reported locations of 0.375-in. (10 mm) and marble-sized hail are shown with numbered dots. Corresponding times are 1) 2130, 2) 2135, 3) 2148, and 4) 2148 UTC. The aircraft location at 1-min intervals is shown by connected dots. North is toward the top of the figure.

itation event, precipitation type, mean and maximum size of hailstones, number density of deposited stones, comments regarding composition and shape, and photographs of the hail. Similar information was provided by a network of volunteer hail observers (some 50 in all), who were recruited from science classes at local high schools. Participants submitted reports for all precipitation events. Hail reports received by the National Weather Service (NWS) were also available.

During 1992 in-cloud measurements of particle distributions were made by the T-28 armored aircraft operated by the South Dakota School of Mines and Technology. Aircraft instrumentation and a summary of the data collected are described in a technical report (Detwiler et al. 1993). On 24 June, a total of eight storm penetrations were made at heights near 3 km. Radar reflectivity along the flight path at times exceeded 60 dBZ, and strong vertical drafts were encountered. Hail was observed on seven of the eight penetrations. Measurements of interest include the reverse flow temperature, the vertical wind speed, the Johnson–Williams liquid water (the concentration of cloud droplets smaller than  $30\text{-}\mu\text{m}$  diameter), the shadow images generated by the Particle Measuring Systems (PMS) Inc. 2D cloud probe (particles  $\geq 25\text{ }\mu\text{m}$  diameter), the Wil-

liamson Foil Impactor (for particles 1–20 mm), and the number counts of the hail spectrometer (particles from 4.5 to 45 mm in diameter). The width of the region sampled by the PMS 2D cloud probe is  $80\text{ }\mu\text{m}$ . However, the diameter of elliptical and circular particles larger than  $80\text{ }\mu\text{m}$  can be estimated from the length and curvature of the shadow images. Vertical velocities were determined from changes in aircraft acceleration and pitch (Kopp 1985).

Event times are not recorded on the foil impactor. Instead, timing is determined from turn-on and turn-off times. The foil is exposed at a rate of 1.5 in. or 38 mm ( $\pm 5\%$ ) each second (A. Detwiler 1993, personal communication). Thus, approximate event times are found by measuring the total amount of foil exposed. Examination of the foil and radar information dictated that, for the pass described here, 20 s should be subtracted from the estimated times for the foil impactor.

At times, the hail spectrometer recorded numerous particles as large as 45 mm. Surface reports, cloud probe images, foil impactor images, radar reflectivity measurements, and dual-wavelength radar measurements all argue that the largest hail was marble sized. Number concentrations detected by the hail spectrometer and the foil impactor are roughly the same. The reason for the size discrepancy is not known. On occasion, the instrument failed altogether and no particles were recorded. The spectrometer data are used qualitatively to indicate regions where large particles were likely.

### c. Computations with the T-28 foil data

To verify the multiparameter radar signatures, the number of solid ice particle (graupel and hail) and raindrop impressions recorded by the foil impactor were tabulated for each 10-s interval in size categories of 1 mm. The imaging surface of the impactor is  $38\text{ mm} \times 38\text{ mm}$ . Multiplying the surface area by the air speed of the aircraft and by 10 s gives the sampling volume  $V_s$ . For example, at a speed of  $92\text{ m s}^{-1}$ ,  $V_s = 1.33\text{ m}^3$ . The radar reflectivity at horizontal polarization for the raindrops is

$$Z_{H,\text{rain}} = \frac{1}{V_s} \sum_{i=1}^n n(D_i) D_i^6 \text{ mm}^6 \text{ m}^{-3},$$

where  $n$  is the number of particles in each size interval per 10 s and  $D_i$  is the mean horizontal axis in the interval. Following Jameson (1983), the reflectivity at vertical polarization was computed from

$$Z_{V,\text{rain}} = \frac{1}{V_s} \sum_{i=1}^n n(D_i) r(D_i)^{7/3} D_i^6 \text{ mm}^6 \text{ m}^{-3},$$

where the equilibrium axis ratio  $r [= 1.03 - 0.062D_i]$  is an empirically derived adjustment for the reduction in the vertical axis of raindrops due to flattening.

It is assumed that the axes of the ice particles were nonaligned; hence, the radar reflectivity for the ice particles was

$$Z_{\text{ice}} = \frac{1}{5.28 V_s} \sum_{i=1}^n n(D_i) D_i^6 \text{ mm}^6 \text{ m}^{-3},$$

where the constant 5.28 (see Smith 1984) accounts for the lower dielectric constant of pure ice having a density of  $0.917 \text{ g cm}^{-3}$ . [With lower bulk densities the reflectivity is lower (Vivekanandan et al. 1994, p. 2).] With this partitioning of the rain and ice particles, the differential reflectivity becomes

$$Z_{\text{DR}} = 10 \log \left( \frac{Z_{H,\text{rain}} + Z_{\text{ice}}}{Z_{V,\text{rain}} + Z_{\text{ice}}} \right) \text{ dB}$$

when reflectivity is expressed in the usual units ( $\text{mm}^6 \text{ m}^{-3}$ ).

The diameter of all foil images ( $D_{\text{img}}$ ) were corrected for the bloom that occurs when they strike the sensor. The relationship used, found by applying a linear least squares fit to the data in Figs. 6 and 7 of Schecter and Russ (1970), was

$$D_i = 0.89 D_{\text{img}}.$$

#### d. Precipitation particle model

To interpret the observations and to check the dataset for consistency, a dual-Doppler wind field analysis was used to initialize the precipitation growth model of Knight and Knupp (1986). Temperature and moisture profiles were obtained from an environmental sounding. The model, which assumes that the wind field is steady, is used to evaluate possible source regions for hail embryos and to determine likely hailstone trajectories. Although several model configurations were tested, only results thought representative of the low-density hail frequently observed in northeastern Colorado (case II of Knight and Knupp) are presented here. The density of ice particles  $\rho_i$  ( $\text{g cm}^{-3}$ ) is given by

$$\rho_i = 0.211R + 0.489,$$

where  $R$  (cm) is the particle radius. Terminal velocities  $v_t$  are computed (following Macklin 1977) from

$$v_t = \left( \frac{8g}{3C_D} \frac{\rho_i}{\rho_a} R \right)^{1/2},$$

where  $\rho_a$  is the density of air,  $g$  is the acceleration due to gravity, and  $C_D$  is the drag coefficient (set to 0.75). The collection efficiency in the model is unity. Liquid water amounts are adiabatic for vertical velocities  $w > 10 \text{ m s}^{-1}$  and linearly decrease to zero as  $w$  approaches 0. The storm glaciates between temperatures of  $-20^\circ$  and  $-40^\circ\text{C}$ . Growth is not permitted at temperatures above  $0^\circ\text{C}$ .

### 3. Observations from 24 June 1992

The storm complex developed in the early afternoon over the mountains and moved onto the plains after 2000. [Environmental conditions and an overview of storm evolution are given by Bringi et al. (1995).] Many storm features were similar to those described by Nelson (1987) for "hybrid multicellular–supercellular" hailstorms. In particular, the 24 June storm was characterized by a large overhang (seen in vertical cross sections made by the CP-2 radar, not shown), a large region of moderate updrafts with multiple centers, an outflow boundary along which new cells formed, and an elongated zone of high reflectivity that was roughly parallel to the outflow boundary.

Figure 3 depicts the storm at 2137. Previously, heavy rain and copious amounts of marble-sized hail had fallen in Fort Collins, Colorado (reports 1 and 2, Fig. 3). Curious storm features include three reflectivity bands marked in Fig. 3. The central band had a lifetime of only 30 min. The northernmost band (the "feeder band") persisted for more than 1.5 h maintaining maximum radar reflectivity of 40–50 dBZ. The feeder band remained quasi-stationary as the storm propagated southeastward at about  $1 \text{ m s}^{-1}$ . This band may have been a major source of hail embryos (section 3c). Storm propagation was along the southernmost band, which persisted for more than 1 h. The spiral-like pattern of the reflectivity bands, surface wind observations, and environmental soundings hint that a mesoscale circulation of about 100 km in diameter accompanied the storm.

Although the aircraft penetrated the storm eight times between 2130 and 2300, only data from the first pass are described here. The aircraft approached from the south entering the storm core—that is, the region with reflectivity of at least 40 dBZ—at 2136:45 (Fig. 4). A slight turn was made toward the north-northeast before exiting the core. Afterward the aircraft crossed a weak reflectivity region and passed through the feeder band.

#### a. Storm morphology

A dual-Doppler analysis at 3 km for that portion of the storm complex penetrated by the aircraft is presented in Fig. 4. (Figure 3 shows the location of the analysis with respect to the storm complex.) Below 1 km, strong winds approached the storm from the northeast (not shown). The linear momentum of this flow is retained in updraft maxima at 3 km, suggesting that the northeasterly winds were the primary inflow source for the storm. The aircraft penetrated the updraft near  $x = 24$ ,  $y = 73 \text{ km}$  between 2139:00 and 2140:00.

Vertical cross sections through the storm (e.g., Fig. 5) support the notion that the storm inflow is principally from the northeast. Updrafts have their roots in the reflectivity gradient at low levels and tilt south-

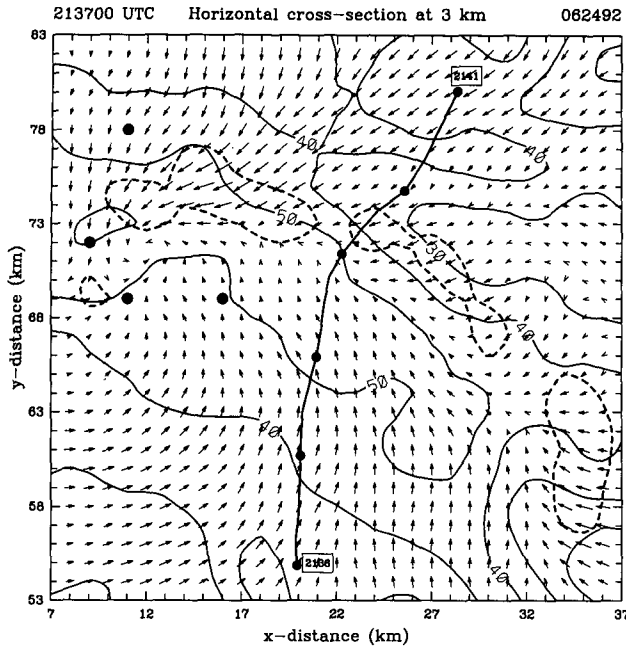


FIG. 4. Dual-Doppler radar analysis at 3-km elevation (above ground level) showing the storm-relative horizontal wind field in the 24 June 1992 thunderstorm complex (2137 UTC). A vector 1 km in length (one grid space) represents  $20 \text{ m s}^{-1}$ . Contours are radar reflectivity from the CP-2 radar at 10-dBZ intervals. Updrafts greater than  $10 \text{ m s}^{-1}$  are enclosed by dashed lines. Distances are from the CP-2 radar. The aircraft track is shown by a series of connected dots spaced at 1-min intervals and beginning at 2136 UTC (southernmost point). The large dots correspond to the hail reports in Fig. 3.

westward over the high-reflectivity region with height. Environmental soundings and aircraft measurements indicate that the freezing level was approximately 3 km. Ambient air from the south (left) tends to sink upon entering the storm (Fig. 5). Except near  $y = 57.6$ ,  $z = 2$  km, there is no indication of a radar reflectivity bright band below the melting level. There are, however, multiparameter radar signatures for melting (section 3b).

The aforementioned quasi-stationary band of enhanced radar reflectivity, visible in Figs. 4 and 5 ( $x = 26.6$ ,  $y = 76.5$  km), resides on the inflow side of the storm. Tops of 40-dBZ cells within the band were less than 8 km and distinctly separate from the overcasting storm anvil. Updrafts associated with this shallow convection (e.g., Fig. 5) are relatively weak compared to those of the main storm.

Aircraft-measured vertical velocities are shown in Fig. 6b. For comparison purposes, radar-derived vertical velocities interpolated to the aircraft's location are superimposed (the smooth curve). The agreement is fair. There is a 10–15-s (roughly 1.5 km) offset between the radar-derived and aircraft-sensed updraft maxima. Other differences exist in the strong inflow to the storm (probed by the aircraft between 2140 and 2141). The storm's relatively poor position for dual-

Doppler analysis, the unsteadiness of small storm features, and the differential motion of the updraft penetrated relative to that of the storm complex are all likely contributors to the discrepancies. The differences restrict conclusions that can be drawn from the direct comparison of the radar and in situ measurements.

Aircraft measurements from 2136:00 to 2138:35 confirm that the southwestern flank of the storm complex was dominated by downdrafts (Figs. 5 and 6b). As the aircraft crossed the axis of maximum reflectivity, downdrafts slowly decreased. Large velocity variance from 2138:50 to 2139:10 may relate to mixing between the subsiding and rising currents.

As noted, strong updrafts observed from 2139:00 to 2140:00 roughly coincide with those in the radar analysis. Peak drafts measured by aircraft were almost  $18 \text{ m s}^{-1}$  (2139:31). The general region of updrafts sensed by the aircraft exhibited small-scale variations including downdrafts not seen in the radar analysis. That the fluctuations were real is suggested by their correspondence with similar variations in temperature and cloud water content (Figs. 6c,d). Importantly, some particles would fall through the general region of aircraft-sensed updrafts, while the same-sized particles would be swept upward by the radar-derived updrafts.

Aircraft-measured temperatures on the storm's southern flank were generally above freezing and did not fall below  $0^\circ\text{C}$  permanently until 2137:52, approximately when the plane entered the region with reflec-

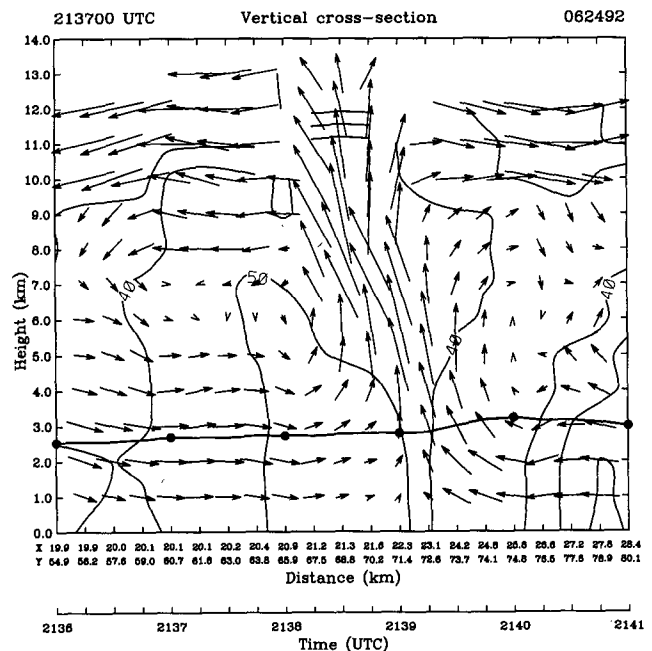


FIG. 5. Vertical cross section of radar reflectivity and radar-derived winds along the aircraft track. A 1-km distance corresponds to  $10 \text{ m s}^{-1}$ . The width of the figure represents the period from 2136 to 2141 UTC. Columns are spaced at 15-s intervals; coordinates are relative to the CP-2 radar.

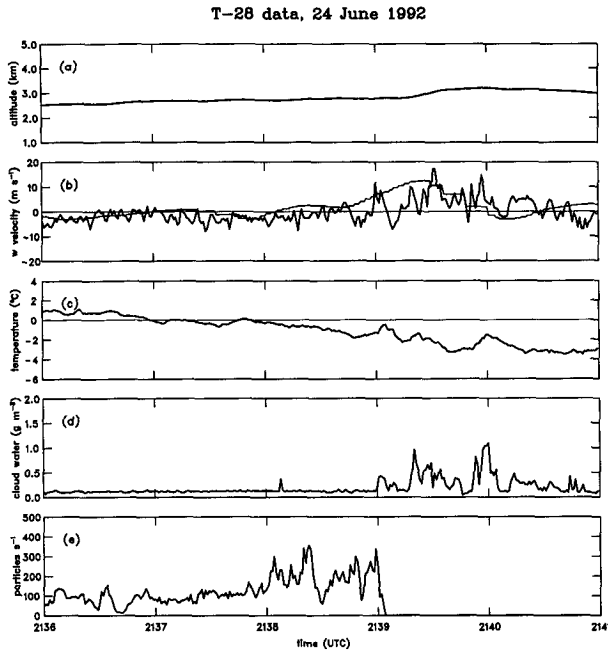


FIG. 6. (a) Traces of aircraft altitude, (b) updrafts, (c) dry-bulb temperature, (d) liquid cloud water, and (e) total number of particles observed with the hail spectrometer as determined with the T-28 between 2136 and 2141 UTC 24 June 1992. Measurements are plotted at 1-s intervals; heights are AGL. The hail spectrometer malfunctioned shortly after 2139:00 UTC. For comparison, updrafts determined by dual-Doppler analysis and interpolated to the aircraft's location are superimposed on (b) (the smooth trace).

tivity greater than 50 dBZ. The general cooling responds in large part to an increase in aircraft altitude (Fig. 6a).

#### b. Examination of the multiparameter radar measurements and in situ particle observations

##### 1) THE REFLECTIVITY CORE

Multiparameter radar measurements projected onto a horizontal plane close to the mean height of the aircraft (3 km) and to a vertical cross section along the aircraft's path are presented in Figs. 7 and 8. At 3 km,  $Z_{DR}$  throughout much of the reflectivity core (the region of greater than 40 dBZ) was small and often negative (Fig. 7a). The region of small absolute differential reflectivity was bounded on its north and east by a distinct belt of large  $Z_{DR}$ . Figure 8a shows that early in the flight the aircraft traveled close to the base of the near zero  $Z_{DR}$  zone and that  $Z_{DR}$  increased steadily below 3 km.

The 2D cloud probe images obtained on the storm's southern flank during the period 2136:35–2138:35 (not shown) depict numerous irregularly shaped ice particles smaller than 0.8 mm in dimension but no raindrops. Tumbling frozen particles with nonaligned major axes would cause a  $Z_{DR}$  of zero; a slight preference for the major axis to be aligned vertically in the mean

seems the most likely cause of the small negative values. However, modeling studies by Aydin and Seliga (1984) reveal that wet conical graupel with diameters less than 0.8 mm could produce a negative  $Z_{DR}$ . Flight-level dry-bulb temperatures decreased from +0.9°C at 2136:35 to -0.7°C at 2137:35 (Fig. 6c). A slight warming to +0.1°C occurred until 2137:49 when temperatures began to fall again. Wet-bulb temperatures were probably a little colder. Some small wet graupel may have been associated with the assumed bright band ( $y = 60.7$ ,  $z = 3$  km, Fig. 8a). The increase in  $Z_{DR}$  toward ground is clearly due to melting.

The maximum size of ice particles detected by the 2D cloud probe grew slowly along the aircraft's path through the storm core. The number of particles larger than 4.5 mm detected by the hail spectrometer also increased (Fig. 6e), but concentrations were highly variable, particularly from 2138:00 until the instrument failed at 2139:04 (Fig. 6e). A hail stone estimated to be 10 mm in diameter was observed with the cloud probe at 2138:07. Another stone 12 mm in diameter was detected at 2138:25. Both stones were close to the axis of maximum reflectivity. Afterward, maximum sizes decreased. Two stones of 8 mm were found at 2138:39, and one of 7 mm was observed at 2138:54. The maximum size of detected particles remained less than 5 mm until 2140:16 when a 6.5-mm particle was found in the feeder band. At the height of the aircraft, melting within the storm was minimal; and the  $Z_{DR}$  parameter does not distinguish between the small, irregularly shaped particles observed early in the flight and the hail stones found in the storm core (Fig. 8a). The sharp downward turning of differential reflectivity contours that occurs below 3 km between  $x = 20.4$  and 20.9 km and the upward turning of the contours at  $x = 21.6$  km defines a hail shaft of about 5 km in width. The  $Z_{DR}$  minimum and gradients are fairly typical (e.g., Bringi et al. 1986).

The distribution of particles observed with the foil impactor is presented in Fig. 9. No attempt has been made to distinguish between graupel and hail, except that particles larger than 5 mm are considered hail. The foil data reveal that the total number of ice particles increased slowly from 2136:00 until 2138:40. Several hailstones of 13 mm were recorded in the 10-s intervals centered at 2138:03 and 2138:13. Stones of at least 10 mm were observed only within the region of at least 50 dBZ and only from 2137:58 to 2138:48 (Fig. 4). The stones resided beneath the sloping updraft (Fig. 5). Local winds would have carried the stones northwestward back toward the updraft arc before impact at ground.

Radar reflectivity and differential reflectivity computed from the foil images and interpolated from the radar measurements to the aircraft's location are displayed in Figs. 10a,b. Agreement is excellent considering the differences in sample volume and the simplifying assumptions used in the calculations (section

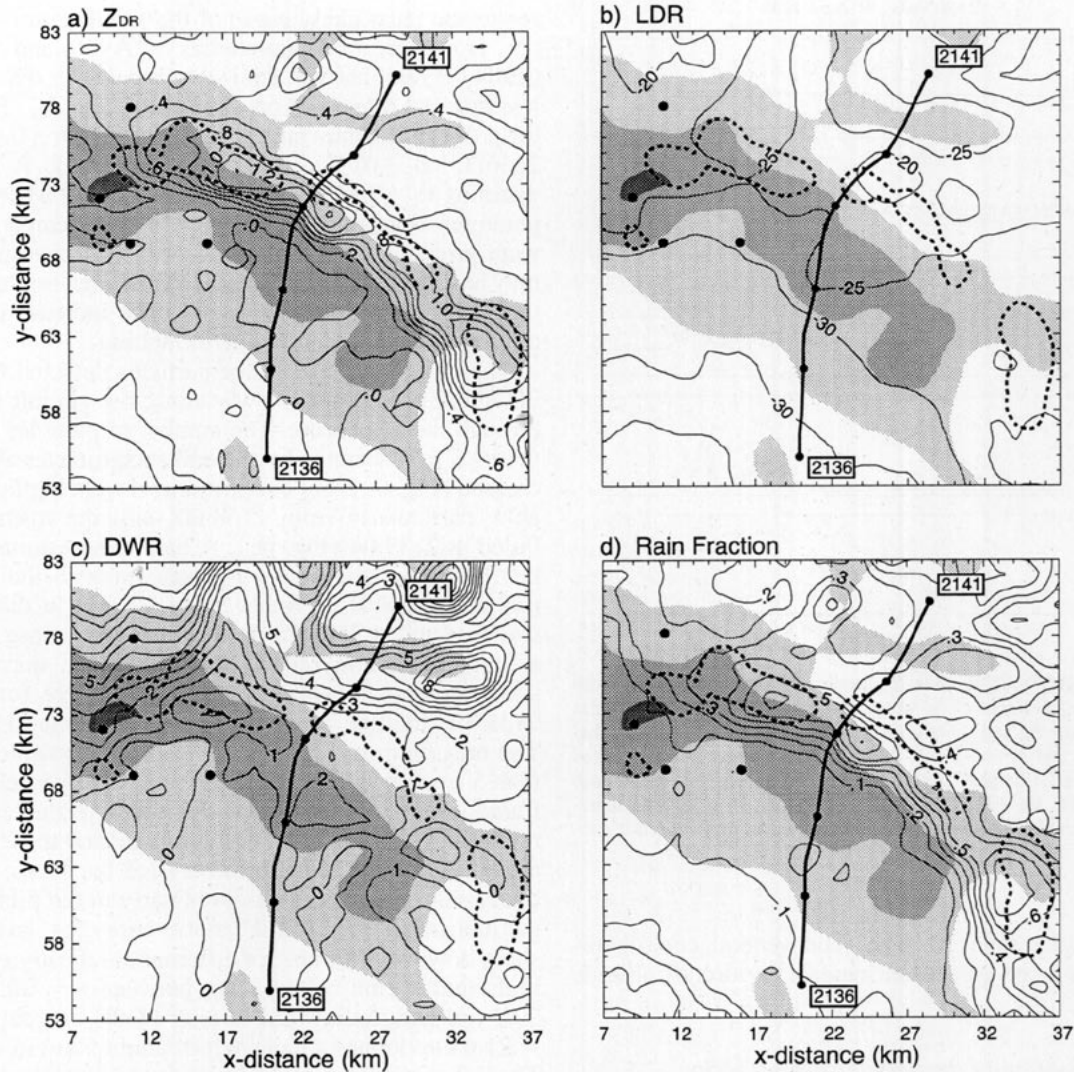


FIG. 7. Multiparameter observations at 3 km AGL obtained at 2137 UTC 24 June 1992 with the CP-2 radar. Displayed variables include (a) the differential reflectivity, (b) the linear depolarization ratio, (c) the dual-wavelength ratio, and (d) the rain fraction. The analysis domain and overlays are as in Fig. 4. The radar reflectivity field is stippled at 10-dB steps beginning at 40 dBZ.

2c). The computed reflectivity maximum of 60 dBZ closely matches the radar-measured reflectivity maximum in magnitude. Differential reflectivity calculated from the impactor data is essentially zero throughout the period 2136:00–2138:40. This is to be expected because raindrops were generally absent and because ice particles were assumed to fall with nonaligned axes. In truth, the few small raindrops designated between 2136:00 and 2137:43 (Fig. 9a) may have resulted from an inability to distinguish between small liquid and small frozen drops (Knight et al. 1976).

From 2136:35 to 2137:45 the aircraft passed through a region where the linear depolarization measurements averaged approximately  $-30$  dB (Figs. 7b, 8b). LDR values of this magnitude associate with small droplets

and pristine ice crystals (Table 1). Neither particle type was detected by the 2D cloud probe along the southern flank of the storm. Instead, numerous small, asymmetric ice particles, thought to be precipitation debris, were observed. Maximum particle sizes increased with time, an indication that a size-sorting mechanism was operating. An increase in mean size is consistent with both the increase in reflectivity and the increase in LDR between 2137:00 and 2138:00. The slight increase in LDR toward ground could result from melting and the accretion of droplets.

While in the storm's reflectivity core, the aircraft passed through the western portions of a region with  $LDR > -25$  dB. Because the antenna elevation angle for viewing is small and the reflectivity is strong, pris-

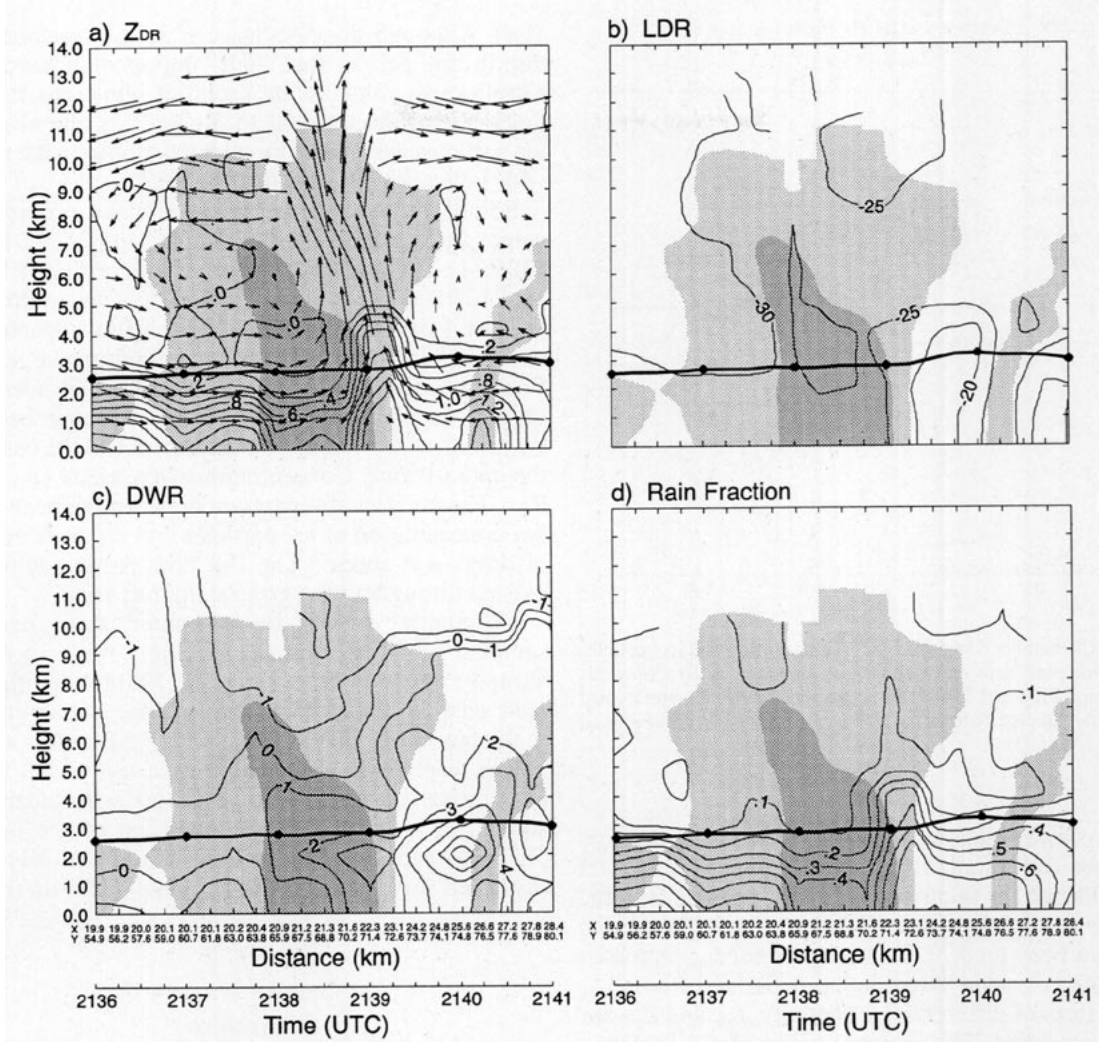


FIG. 8. Multiparameter observations as in Fig. 7 but for a vertical cross section along the aircraft track. Radar reflectivity and winds are selectively superimposed.

tine ice crystals are ruled out as the dominant particle type. High reflectivity also makes it unlikely that small drops or aggregates are dominant. Because  $Z_{DR}$  is slightly negative, the presence of large drops is unlikely. Thus, a mixture of graupel and hail particles is inferred (Vivekanandan et al. 1993). The region of large LDR extends above the melting level to more than 5 km and is directly above the  $Z_{DR}$  hail signal at low levels. Consequently, LDR provides a signature for hail above the melting layer (Bringi et al. 1986).

Dual-wavelength measurements are pictured in Figs. 7c and 8c. To the right of the aircraft track, where LDR was large, a small region exists with dual-wavelength ratios of 2–3 dB. Particle sizes in this region should be a little larger than along the flight path. The maximum diameter of the observed hail is somewhat larger than expected from the DWR parameter. The fact that  $Z_{DR}$  is slightly negative in the region of large DWR is evi-

dence that the hailstones were probably dry (Table 1) or that their major axes were aligned vertically in the mean.

The region of negative DWR below 2-km elevation (Fig. 8c) is thought to result from sensitivity to ground targets at S band. Evidence for radar signal blockage at low antenna elevations includes several features that are elongated along rays from the CP-2 radar. The most likely explanation for the large domain of  $DWR < -1$  dB above 3.5 km is that there is a systematic calibration bias. If true, the actual DWRs in the hail region may be larger than measured.

The remaining field displayed in Figs. 7d and 8d is the rain fraction. The bias that results in this parameter due to the loss of statistical information (section 2a) is readily apparent. The range of numbers is approximately 0.1–0.8. On the southern edge of the storm and at the altitude of the aircraft  $f_{rain}$  was 0.2–0.3, suggest-

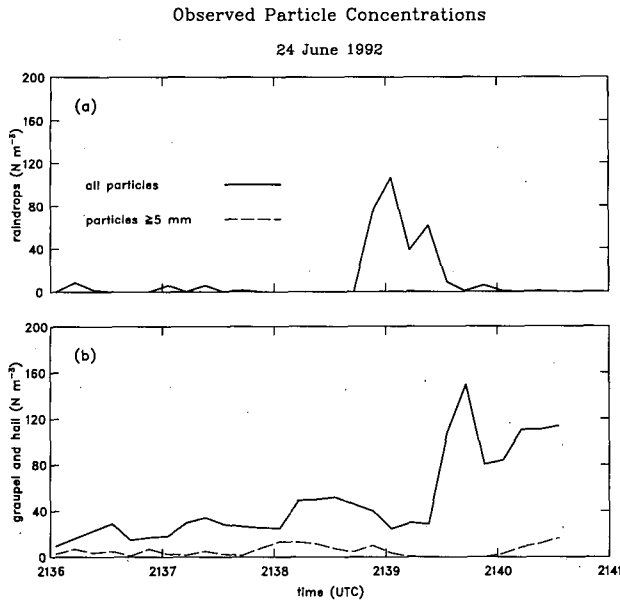


FIG. 9. The number concentration ( $N$ ) of raindrops and ice particles (graupel and hail) detected with the foil impactor in 10-s intervals for the period 2136 and 2141 UTC. The upper solid and lower dashed curves show the distributions for all particles and particles of at least 5 mm.

ing that some water was present. Other than the few suspicious foil impressions mentioned earlier, there is little evidence for raindrops here, but because temperatures were slightly above  $0^{\circ}\text{C}$ , partly melted particles may have been present. Toward ground,  $f_{\text{rain}}$  increases as melting pervades. Because  $f_{\text{rain}}$  is derived from  $Z_{\text{DP}}$ , another form of differential reflectivity,  $f_{\text{rain}}$  and  $Z_{\text{DR}}$  are highly correlated. The intrinsic value of  $f_{\text{rain}}$  is that it can be used to estimate reflectivity-weighted fractions of ice and water. However, the ratio of water and ice concentrations, which depends upon the number and size of the particles, is not known.

## 2) THE STORM UPDRAFT

The aircraft penetrated a general region of updrafts from 2139:00 to 2140:04. Immediately upon entry, significant concentrations of cloud water, intermittently exceeding  $0.5 \text{ g m}^{-3}$ , were detected (Fig. 6d). Peak concentrations were coincident with updraft maxima. Raindrops were first detected with the 2D cloud probe at 2139:00 and with the foil impactor in the 10-s interval 2138:48–2138:58 (Fig. 9a). At 2139:30 the pilot remarked that strong updrafts and “hail” were encountered. No mention was made of size. Foil impactor images (Fig. 9b) show a large increase in the number of ice particles detected between 2139:28 and 2139:38 followed by a maximum at 2139:43. However, nearly all the particles were small (less than 2.5 mm in diameter), and consequently, they had little effect on either the computed or measured radar reflectivity (Fig.

10a). Although stones as large as 5 mm were observed during this period, the “hail” report may have been simply recognition of the sound of numerous ice particles hitting the windshield. Regardless, the observed ice particles were much smaller than those in the region with reflectivity greater than 50 dBZ.

Raindrops, as observed with the cloud probe, often came in bunches—for example, at 2139:01 and 2139:31. The largest drops were bigger than 2.5 mm (at 2139:09, 2139:17, and 2139:22). Twelve drops of at least 4 mm were detected by the foil impactor between 2138:48 and 2139:18, and two drops larger than 5 mm were observed. The largest drops resided in a region roughly bounded by the mixing zone between east-northeasterly and southerly flows and the center of the updraft zone. Concentrations were small (e.g., Fig. 9a). The horizontal separation between the peak number concentration of ice particles and the peak number of drops was about 3 km. But both particle types coexisted throughout the general updraft zone.

Differential reflectivity computed from particles sampled with the impactor (Fig. 10b) increased abruptly between 2138:53 and 2139:03 when the aircraft entered the updraft. The increase is due entirely to the presence of rain (section 2). Peak computed  $Z_{\text{DR}}$  values were 2 dB. Differential reflectivity then fell to near zero as the aircraft exited the updraft. Radar measured  $Z_{\text{DR}}$  also increased at the edge of the updraft (Figs. 8a and 10b). Maximum values (1.2 dB) were displaced slightly southwest (downwind) from the up-

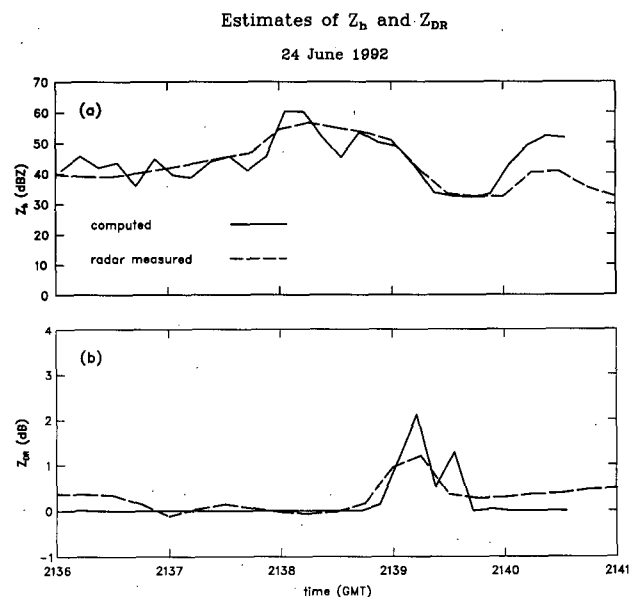


FIG. 10. Computed radar reflectivity at (a) horizontal polarization  $Z_h$  and (b) differential reflectivity  $Z_{\text{DR}}$  using particle distributions determined with the foil impactor (solid lines). Radar-measured values, simple averages of all measurements within 1 km of the aircraft's location, are also shown (dashed lines).

draft maximum (Fig. 7a). The region of positive  $Z_{DR}$  extended well above the freezing level to 5 km.

The association between the  $Z_{DR}$  column and the updraft in Fig. 8a implies a vertical transport of raindrops from low levels. Evidence for the recycling of rain also appears in aircraft and radar data collected between 2155 and 2200 (Bringi et al. 1995). The recycling process seems identical to that computed by Ziegler (1988) in a kinematic microphysical retrieval study of a convective storm (his Fig. 8). The kinematic model also showed a recycling of graupel–hail and rain–hail mixtures at the flanks of the updraft. This can be inferred in the 24 June storm from the deep layer of convergence and the low  $Z_{DR}$  values at the sides of the updraft (Fig. 8a).

At the altitude of the aircraft, LDR exceeded  $-20$  dB in the upwind portions of the updraft (2139:45;  $x = 24.8$ , Fig. 8b), and DWRs grew to more than 4 dB (Fig. 8c,  $x = 25$  km). The DWRs may be a little large given the observed size of the hail. The combination of small  $Z_{DR}$  (0.2–0.3 dB), large LDR, and relatively weak reflectivity signifies small dry hail or graupel (Table 1).

The fractional contribution of rain to radar-measured reflectivity (Figs. 7d and 8d) was a maximum in the updraft core ( $f_{rain}$  is slightly greater than 0.5). In comparison, the rain fraction for the two  $Z_{DR}$  maxima determined from impactor data (Fig. 10b) are 0.82 and 0.75. Considering the number of factors that could contribute to the difference, the agreement is good.

### 3) THE FEEDER BAND

The aircraft passed through the feeder band between 2140 and 2141. Raindrops were not detected by either the 2D cloud probe or the foil impactor. The most common particles were small frozen fragments, but there were some large frozen particles as well. For example, a stone 9.5 mm in diameter was recorded by the foil impactor at about 2140:13. Then there was the 6.5-mm-diameter particle inferred from shadow images obtained with the cloud probe at 2140:16. Other large particles seen by the probe were 5.9 (2140:18) and 5.7 mm (2140:36). Foil impactions (Fig. 9b) reveal that concentrations of all ice particles and large ice particles grew until 2140:33 when the transcription of foil impressions ended.

Radar-measured reflectivity within the feeder band is considerably lower ( $\sim 10$  dB), and  $Z_{DR}$  is higher ( $\sim 0.2$  dB) than that estimated from impactor data. Perhaps, the bulk density of the ice particles in this region of the storm is less than the pure ice density assumed in the calculation of  $Z_{ice}$  (section 2c). Within the reflectivity band, LDR falls to less than  $-26$  dB, and DWR declines from 5 to 3 dB. The tendency for LDR and DWR to increase along the northern flank of the storm is suggestive of sidelobe or signal propagation problems. However, the in situ measurements disclose

that the large DWR measurements between the storm updraft and the feeder band were due, at least in part, to hail.

### c. The source and growth of hail embryos

Possible histories of hailstone development were produced by the precipitation growth model. Figures 11a,b summarize the final size and location of particles beginning at 3-km elevation and having an initial diameter of 2 mm. This size roughly corresponds to the more common particles observed in the updraft and feeder band.

Many embryos for the larger modeled stones originate in a broad region that is roughly centered on the updraft penetrated by the aircraft. Embryos that begin within the updraft maximum (the region with  $w > 10$  m s $^{-1}$ ) attain final diameters of 6–11 mm. Modeled stones with the largest final diameters (19 and 20 mm) start in the reflectivity and vertical velocity gradients behind the axis of strongest updrafts. The region of embryos experiencing large growth extends more than 5 km upwind to the reflectivity gradient along the southern flank of the feeder band. Final sizes of 16–18 mm are indicated for some of these embryos. Interestingly, the 20-mm particle that begins just to the rear of the updraft (Fig. 11a,  $x = 26$ ,  $y = 71$  km) and the 18-mm stone that begins in the feeder band ( $x = 32$ ,  $y = 74$  km) are deposited at roughly the same location (Fig. 11b,  $x = 18$ ,  $y = 72$  km).

The upwind extension of the hail embryo region has the ‘‘embryo corridor’’ appearance described by Nelson (1983) and Ziegler et al. (1983), and hence, the term ‘‘feeder band’’ has been used in reference to this feature. The cessation of surface hail reports once the storm moved away from the band is additional evidence—albeit circumstantial—of its importance to hail production. A difference here from the Nelson and Ziegler et al. studies is that the embryos injected into the 24 June storm’s updraft begin at much lower levels. The general agreement in the size of modeled hailstones and surface reports, which points to the coherence among the radar-derived wind field, the observed reflectivity field, and the precipitation growth model, is gratifying since no special fiddling of model parameters was performed. The loss of the small-scale features in the radar analysis and the assumption that the storm is steady do not appear to have unduly influenced the ensemble of modeled trajectories (Knight and Knupp 1986).

Trajectories for 2-mm hail embryos beginning in the reflectivity gradient on the southern side of the feeder band are presented in Fig. 12. Displayed particles descend initially (up to 1 km) because their terminal velocities exceed the weak ambient vertical drafts (Fig. 12b). Growth ensues when the embryos enter stronger updrafts and rise above the freezing level (3 km). Although some growth occurs in the lower updraft, the

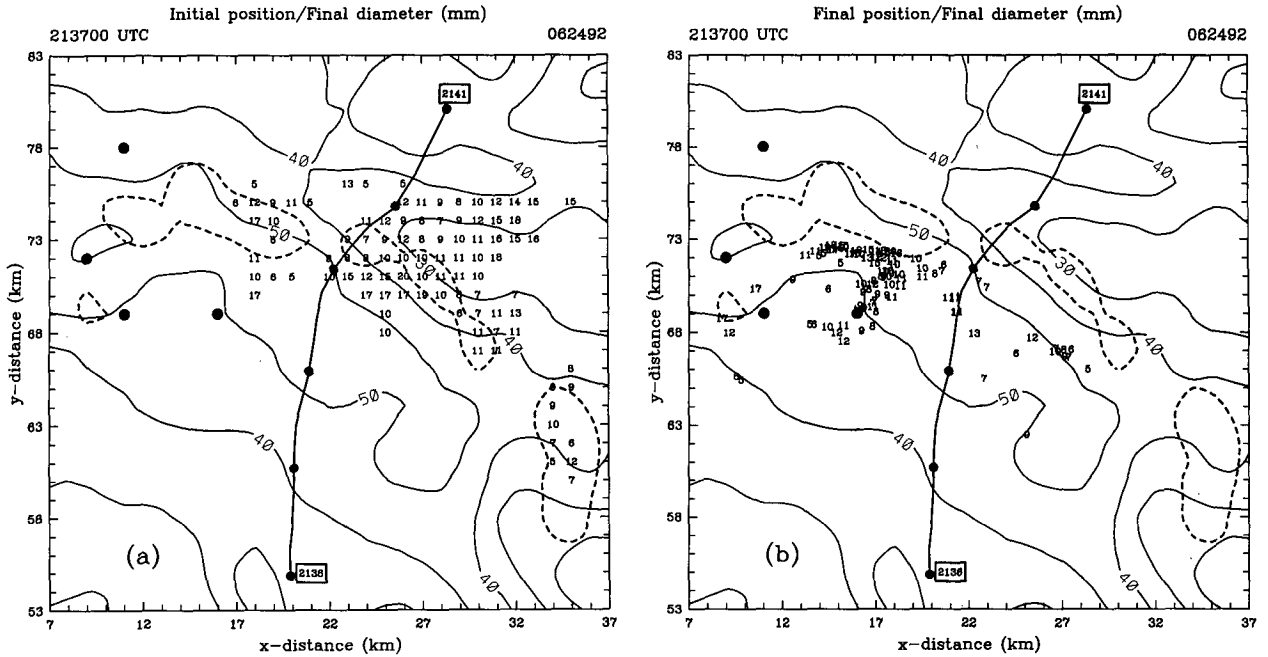


FIG. 11. The final size (mm) of hailstones grown by the model of Knight and Knupp (1986). Panel (a) shows the final size encoded at the initial location of the trajectory, and (b) shows the final size encoded at the point of surface deposition. The initial embryo size was 2 mm, and the initial height was 3 km (AGL). Only embryos experiencing growth and not exiting the analysis domain are shown.

total mass accumulated is relatively small. In fact, none of the stones attain diameters of 5 mm until they rise above 6 km. This is about 7% of the total volume for

a stone with a final diameter of 12 mm. Hail growth is retarded in the lower updraft because particle terminal velocities are relatively small compared to the updraft

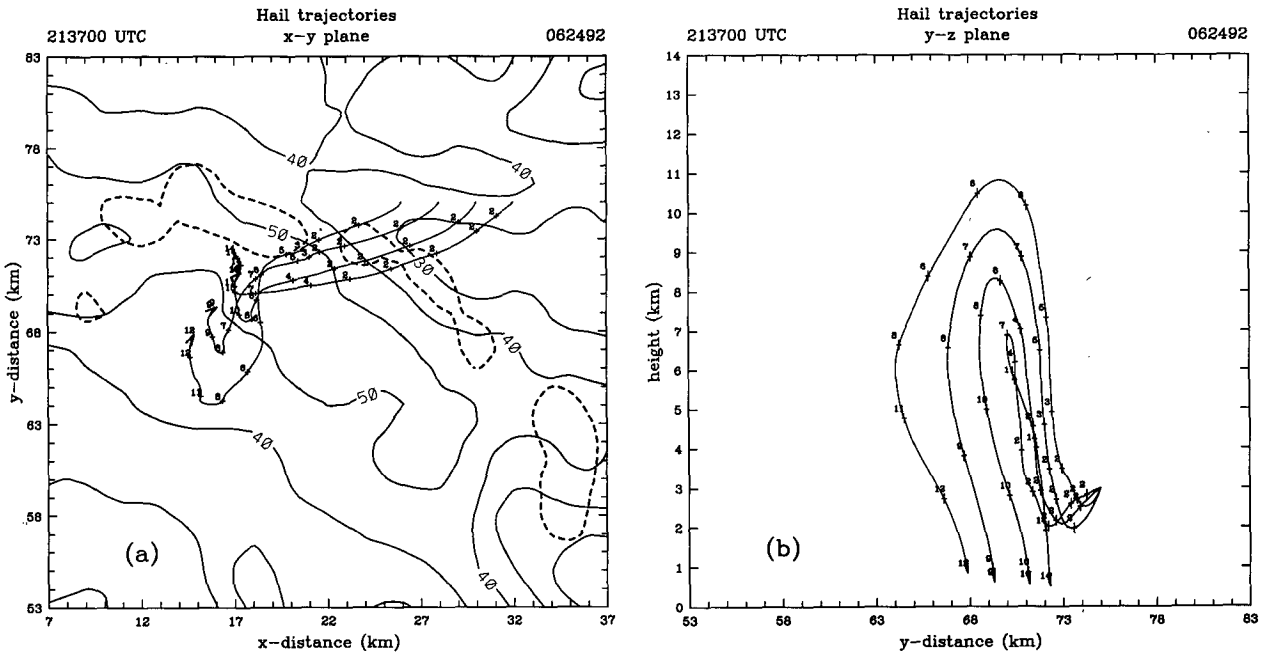


FIG. 12. (a) Plan and (b) north-south projections showing paths and growth histories of selected 2-mm hail embryos originating at 3 km AGL in the feeder band. Sizes are in millimeters; tick marks are at 2-min intervals.

velocity resulting in a short residence time and because concentrations of condensed adiabatic water are relatively small.

All stones in Fig. 12b attain diameters of 6–7 mm and heights of 7–11 km before descending. Much of the growth takes place as the stones fall. The increase in reflectivity between the sloping updraft and the melting level is a manifestation of this growth. Final deposition of many large stones occurs at the edge of another updraft center (near  $x = 17$ ,  $y = 72$  km; Fig. 11b). All modeled stones with diameters of at least 10 mm fall within the observed area of reflectivity of 40 dBZ or greater, and most fall within the bounds of the 50-dBZ area. Ziegler et al. (1983) and Nelson (1983) note that weak horizontal winds favor hail growth by slowing the advection across the updraft. In the 24 June storm, stones falling from the sloping updraft enter an underlying region of relatively weak horizontal flow near the axis of maximum reflectivity (Fig. 4). The flow carries the hail back toward the updraft (Fig. 12b). Consequently, the deposition zone for the larger stones is only 5 km in width and roughly parallel to and roughly equal in length to the updraft arc (Fig. 11b).

The terminal velocity of 2-mm embryos originating within the central and northern portions of the feeder band is large enough that they fall to the ground before encountering strong updrafts. Embryos that begin within the storm core and grow to large size originate close to the updraft arc. Horizontal advection behind the arc was relatively weak compared to that feeding into the storm from the northeast (Fig. 5). Consequently, embryos from the reflectivity core side of the arc were more likely to fall from the storm than be recirculated in the updraft.

Embryos with initial diameters less than 2 mm enter the updraft from a broad region that extends from the axis of maximum reflectivity along the feeder band to several kilometers behind the axis of strong updrafts. Because their terminal velocity is less, small embryos are more likely to exit the data domain or the updraft before large growth occurs. Embryos that begin at lower levels and experience growth tend to originate close to the axis of maximum updrafts. Embryos from the “hail” region reported by the pilot at 2139:30 ( $x = 24$ ,  $y = 74$  km) also exhibit significant growth. Diameters less than or equal to 10 mm are predicted before deposition within the same general area as the stones in Fig. 12. Of the 200 or so trajectories that were produced, no hailstones (i.e., particles with diameters of at least 5 mm) were observed to recycle in the updraft.

In summary, in order to be hail embryos, initial size is important. Embryos must be large enough that they do not rise too quickly in the updraft but not so large that they fall from the updraft. The largest stones remained in proximity to the updraft maximum and grew during most of their journey through the storm. As in previous studies, factors that favor growth are those

that increased the dwell time in the updraft—that is, large updraft widths, small absolute differences in the updraft speed and particle terminal velocity, and weak horizontal flow.

#### 4. Discussion and conclusions

A comparison between remotely acquired multiparameter radar measurements (radar reflectivity, differential reflectivity, and the fractional contribution of liquid water to the total reflectivity) showed good agreement with in situ particle measurements made by research aircraft. Radar reflectivity computed from observed particle distributions and measured by radar generally differed by less than 5 dB. Differential reflectivity estimates differed by less than 0.8 dB. The region of large positive  $Z_{DR}$  (the  $Z_{DR}$  column) was closely tied to the updraft and clearly signified the presence of liquid water. Estimates of the proportional contribution of raindrops and ice to the total radar reflectivity, based upon departures from all-rain considerations, were reasonable when the rain proportions were intermediate.

The  $Z_{DR}$  parameter provided an unambiguous hail signature and defined the limits of the hail shaft below the melting level. Measurements of linear depolarization ratio delineated the elevated hail shaft. Dual-wavelength ratios within the reflectivity were about 1 dB smaller than expected for the observed maximum hail size. DWR and LDR, based on measurements at X band, seemed affected by a variety of propagation problems, particularly after the signals passed through the hail and high-reflectivity region.

Aircraft particle measurements confirm that the  $Z_{DR}$  column is characterized by small numbers of large raindrops. This finding was anticipated by Caylor and Illingworth (1987), Tuttle et al. (1989), and Meischner et al. (1991). The origin of the large drops and their importance to hail production is still being established. The presence of  $Z_{DR}$  columns in the early development of isolated cells led Caylor and Illingworth (1987) to suppose that the large drops were caused by warm cloud processes in which giant nuclei swept out cloud droplets as they fell. Illingworth et al. (1987) concluded that melting was not the source of the drops, because the columns in their study did not begin in the melting layer. They also hypothesized that droplet growth was largely by the condensation-coalescence process. However, Foote (1985) has pointed out that in Colorado thunderstorms the condensation-coalescence of cloud material simply takes too long for large drops to form.

Other possible explanations for the large drops are totally or partially melted hail and graupel, drops shed from melting hail, and drops shed by hail undergoing wet growth. For particles originating in the feeder band, drops shed as the result of wet growth can be ruled out because raindrops were not observed in the feeder band

(e.g., Fig. 9a) and cloud liquid water concentrations were relatively low compared to those in the general updraft region (Fig. 6). Laboratory experiments conducted by Rasmussen and Heymsfield (1987, Fig. 1) reveal that melting hailstones smaller than 9 mm in diameter typically do not shed drops. Because observed particles were no larger than 9.5 mm, melted or partially melted hail and graupel seems the most likely explanation for large drops that may have originated in the southern half of the feeder band.

The shedding of drops from melting hail is a possible source for large drops that may have originated in the storm's reflectivity core. The hail was larger in the core, and meltwater shed from hail falling from the underside of the updraft could have been carried back toward the updraft by the low-level southerly flow. Drop shedding from hail undergoing wet growth probably did not occur. Stones observed in the updraft and  $Z_{DR}$  column were too small to shed drops.

Melted ice particles, which fell from the anvil, were thought to compose the  $Z_{DR}$  column in the storm studied by Conway and Zrnić (1993). Tuttle (1993) has described a situation where melted graupel from a large thunderstorm were recirculated in new updrafts at the storm's periphery. The primary source of hail embryos in the 24 June storm may have been the feeder band. Many of the large number of small frozen particles detected upwind from the updraft between 2139:28 and 2139:58 were undoubtedly swept up by the updraft. Meltwater and partially melted particles ingested by the updraft upon refreezing could constitute another embryo source. Model trajectories imply that an important secondary source of embryos may have been the reflectivity core.

Conway and Zrnić (1993) supposed that the  $Z_{DR}$  column and its spatial offset from updraft maximum plays an important role in embryo production and hail growth. They reason that if speeds in the updraft core greatly exceed terminal velocities ( $w \gg v_t$ ) particles rise too rapidly for large growth. Instead, growth occurs in the column where moderate updrafts exist ( $w > v_t$ ). There are reasons to suspect that the portion of the  $Z_{DR}$  column penetrated by the aircraft did not dominate hail growth in the 24 June storm. First, the terminal velocity for drops larger than 2.5 mm in diameter exceeds  $7 \text{ m s}^{-1}$  (Gunn and Kinzer 1949). In situ vertical velocities measured by the aircraft at the time of large drop detection with the cloud probe (e.g., at 2139:09, 2139:17, and 2139:22) varied from  $-7$  to  $+4 \text{ m s}^{-1}$ . The largest drops, those that dominate the  $Z_{DR}$  measurement, would not become hail embryos but would have simply fallen from the storm (the case where  $w < v_t$ ). The drops may have fell from the sloping updraft much like the large hail thereby creating the small offset seen in Figs. 7a and 8a between the axes of maximum updrafts and maximum  $Z_{DR}$ . The implied vertical transport of rain mentioned earlier would have involved only the smaller drops. Second, the supercooled water

concentration of the large drops, as computed from the foil images, averages about  $0.2 \text{ g m}^{-3}$  with a maximum value of  $0.5 \text{ g m}^{-3}$ . In fact, the water concentration, computed from the drops that gave the maximum  $Z_{DR}$  (2.0 dB), was only  $0.19 \text{ g m}^{-3}$ . In contrast, the concentration of cloud water averaged about  $0.4 \text{ g m}^{-3}$  with a maximum value of  $1.03 \text{ g m}^{-3}$ . Thus, the large drops were not the primary source of supercooled liquid water in the lower updraft nor were they likely to have been a deterministic factor for stone growth. Note, however, that in other regions of the storm where  $Z_{DR}$  columns have closer ties to updraft centers (e.g.,  $x = 18, y = 74 \text{ km}$ , Fig. 7a) the mix of particles serving as hail embryos could have been quite different.

Even a cursory examination of the observations and modeling results points to the complexity of hail production in the 24 June storm. The principal updraft region, as observed by aircraft, exhibited small-scale features that included small, weak downdrafts. The updraft (downdraft) perturbations were well correlated with maxima (minima) in cloud water content. Similar corresponding fluctuations were found in the temperature trace. The small-scale variability must leave its imprint in rings of varying ice density as hail embryos grow and broaden the size spectrum of deposited hailstones. A detailed comparison of multiparameter radar measurements and hail ring growth would be an interesting future application.

*Acknowledgments.* The success of the field program was a tribute to many people, but the efforts of several key people require special mention. Nancy Knight established the guidelines for the hail chase teams and served as perpetual driver during 1992. Ben Bernstein served as coordinator for the network of volunteer hail observers. Copies of hail reports received at the National Weather Service office in Denver were graciously provided by Larry Mooney, meteorologist-in-charge. The assistance of Dennis Musil (aircraft meteorologist) and Andy Detwiler (project manager) from the South Dakota School of Mines and Technology is greatly appreciated. We wish to thank Bill Irwin and John Cowins, radar operators, who endured the long days and hours, often when there was little or no activity. The shadow images were produced by Joanne George. Jonathan Smith assisted in the preparation of the figures. The authors are grateful to Charles A. Knight for sharing his expertise in foil image interpretation and to Mark Watson, a participant in NCAR's 1993 Summer Employment Program, who tabulated the image data.

This research is sponsored by the National Science Foundation through an Interagency Agreement in response to requirements and funding by the Federal Aviation Administration's Aviation Weather Development Program. The views expressed are those of the authors and do not necessarily represent the official policy or position of the U.S. Government.

## REFERENCES

- Atlas, D., and F. H. Ludlam, 1961: Multi-wavelength radar reflectivity of hailstorms. *Quart. J. Roy. Meteor. Soc.*, **87**, 523–534.
- Aydin, K., and T. A. Seliga, 1984: Radar polarimetric backscattering properties of conical hail. *J. Atmos. Sci.*, **41**, 1887–1892.
- , —, and V. Balaji, 1986: Remote sensing of hail with a dual linear polarization radar. *J. Climate Appl. Meteor.*, **25**, 1475–1484.
- Battani, L. J., 1973: *Radar Observation of the Atmosphere*. University of Chicago Press, 324 pp.
- Brandes, E. A., 1977: Flow in severe thunderstorms observed by dual-Doppler radar. *Mon. Wea. Rev.*, **105**, 113–120.
- Bringi, V. N., T. A. Seliga, and K. Aydin, 1984: Hail detection with a differential reflectivity radar. *Science*, **225**, 1145–1147.
- , J. Vivekanandan, and J. D. Tuttle, 1986: Multiparameter radar measurements in Colorado convective storms. Part II: Hail detection studies. *J. Atmos. Sci.*, **43**, 2564–2577.
- , L. Liu, P. C. Kennedy, V. Chandrasekar, and S. A. Rutledge, 1995: Dual multiparameter radar observations of intense convective storms: The 24 June 1992 case study. *Meteor. Atmos. Phys.*, in press.
- Caylor, I. J., and A. J. Illingworth, 1987: Radar observations and modelling of warm rain initiation. *Quart. J. Roy. Meteor. Soc.*, **113**, 1171–1191.
- Conway, J. W., and D. S. Zrnić, 1993: A study of embryo production and hail growth using dual-Doppler and multiparameter radars. *Mon. Wea. Rev.*, **121**, 2511–2528.
- Davies-Jones, R. P., 1979: Dual-Doppler radar coverage area as a function of measurement accuracy and spatial resolution. *J. Appl. Meteor.*, **18**, 1229–1233.
- Detwiler, A. G., R. F. Kelley, and P. L. Smith, 1993: Summary Report of T-28 Deployment to Colorado (June 1992). Institute of Atmospheric Sciences, South Dakota School of Mines and Tech. Rep. IAS/R-92/09, 33 pp. plus appendixes.
- Doviak, R. J., and D. S. Zrnić, 1984: *Doppler Radar and Weather Observations*. Academic Press, 458 pp.
- Eccles, P. J., and D. Atlas, 1973: A dual-wavelength radar hail detector. *J. Appl. Meteor.*, **12**, 847–854.
- Foote, G. B., 1985: Aspects of cumulonimbus classification relevant to the hail problem. *J. Rech. Atmos.*, **19**, 61–74.
- Golestani, Y., V. Chandrasekar, and V. N. Bringi, 1989: Intercomparison of multiparameter radar measurements. Preprints, *24th Conf. on Radar Meteorology*, Tallahassee, FL, Amer. Meteor. Soc., 309–314.
- Gunn, R., and G. D. Kinzer, 1949: The terminal velocity of fall for water droplets in stagnant air. *J. Meteor.*, **6**, 243–248.
- Herzogh, P. H., and A. R. Jameson, 1992: Observing precipitation through dual-polarization radar measurements. *Bull. Amer. Meteor. Soc.*, **73**, 1365–1374.
- Illingworth, A. J., J. W. F. Goddard, and S. M. Cherry, 1986: Detection of hail by dual-polarization radar. *Nature*, **320**, 431–433.
- , —, and —, 1987: Polarization radar studies of precipitation development in convective storms. *Quart. J. Roy. Meteor. Soc.*, **113**, 469–489.
- Jameson, A. R., 1983: Microphysical interpretation of multi-parameter radar measurements in rain. Part I: Interpretation of polarization measurements and estimation of raindrop shapes. *J. Atmos. Sci.*, **40**, 1792–1802.
- Keeler, R. J., B. W. Lewis, and G. R. Gray, 1989: Description of NCAR/FOF CP-2 meteorological Doppler radar. Preprints, *24th Conf. on Radar Meteorology*, Tallahassee, FL, Amer. Meteor. Soc., 589–592.
- Knight, C. A., and K. R. Knupp, 1986: Precipitation growth trajectories in a CCOPE storm. *J. Atmos. Sci.*, **43**, 1057–1073.
- , and N. C. Knight, 1970: The falling behavior of hailstones. *J. Atmos. Sci.*, **27**, 672–681.
- , —, W. W. Grotewold, and T. W. Cannon, 1976: Interpretation of foil impactor impressions of water and ice. Preprints, *Int. Conf. on Cloud Physics*, Boulder, CO, Amer. Meteor. Soc., 519–521.
- Kopp, F. J., 1985: Deduction of vertical motion in the atmosphere from aircraft measurements. *J. Atmos. Oceanic Technol.*, **2**, 684–688.
- Macklin, W. C., 1977: The characteristics of natural hailstones and their interpretation. *Hail: A Review of Hail Science and Hail Suppression. Meteor. Monogr.*, No. 38, Amer. Meteor. Soc., 65–88.
- Meischner, P. F., V. N. Bringi, D. Heimann, and H. Höller, 1991: A squall line in Southern Germany: Kinematics and precipitation formation as deduced by advanced polarimetric and Doppler radar measurements. *Mon. Wea. Rev.*, **119**, 678–701.
- Nelson, S. P., 1983: The influence of storm flow structure on hail growth. *J. Atmos. Sci.*, **40**, 1965–1983.
- , 1987: The hybrid multicellular–supercellular storm—An efficient hail producer. Part II: General characteristics and implications for hail growth. *J. Atmos. Sci.*, **44**, 2060–2073.
- Rasmussen, R. M., and A. J. Heymsfield, 1987: Melting and shedding of graupel and hail. Part III: Investigation of the role of shed drops as hail embryos in the 1 August CCOPE severe storm. *J. Atmos. Sci.*, **44**, 2783–2803.
- Ray, P. S., and K. K. Wagner, 1976: Multiple Doppler radar observations of storm. *Geophys. Res. Lett.*, **3**, 189–191.
- Schecter, R. M., and R. G. Russ, 1970: The relationship between imprint size and drop diameter for an airborne drop sampler. *J. Appl. Meteor.*, **9**, 123–126.
- Seliga, T. A., and V. N. Bringi, 1976: Potential use of radar differential reflectivity at orthogonal polarizations for measuring precipitation. *J. Appl. Meteor.*, **15**, 69–76.
- Smith, P. L., 1984: Equivalent radar reflectivity factors for snow and ice particles. *J. Climate Appl. Meteor.*, **23**, 1258–1260.
- Steinhorn, I., and D. S. Zrnić, 1988: Potential uses of differential phase constant to estimate raindrop and hailstone size distributions. *IEEE Trans. Geosci. Remote Sens.*, **26**, 639–648.
- Tuttle, J. D., 1993: Multiparameter radar observations of developing turrets in a high plains storm. Preprints, *26th Int. Conf. Radar Meteorology*, Norman, OK, Amer. Meteor. Soc., 516–518.
- , and R. E. Rinehart, 1983: Attenuation correction in dual-wavelength analyses. *J. Climate Appl. Meteor.*, **22**, 1914–1921.
- , V. N. Bringi, H. D. Orville, and F. J. Kopp, 1989: Multiparameter radar study of a microburst: Comparison with model results. *J. Atmos. Sci.*, **46**, 601–620.
- Vivekanandan, J., R. Raghavan, and V. N. Bringi, 1993: Polarimetric radar modeling of mixtures of precipitation particles. *IEEE Trans. Geosci. Remote Sens.*, **31**, 1017–1030.
- , V. N. Bringi, M. Hagen, and P. Meischner, 1994: Polarimetric radar studies of atmospheric ice particles. *IEEE Trans. Geosci. Remote Sens.*, **32**, 1–10.
- Ziegler, C. L., 1988: Retrieval of thermal and microphysical variables in observed convective storms. Part II: Sensitivity of cloud processes to the variation of microphysical parameterization. *J. Atmos. Sci.*, **45**, 1072–1090.
- , P. S. Ray, and N. C. Knight, 1983: Hail growth in an Oklahoma multicell storm. *J. Atmos. Sci.*, **40**, 1768–1791.
- Zrnić, D. S., N. Balakrishnan, C. L. Ziegler, V. N. Bringi, K. Aydin, and T. Matejka, 1993: Polarimetric signatures in the stratiform region of a mesoscale convective system. *J. Appl. Meteor.*, **32**, 678–693.